OPEN ACCESS

University of BRISTOL

Martin, P. G., Scott, T. B., Payton, O. D., Richards, D. A., Yamashiki, Y., & Fardoulis, J. S. (2016). Low-Altitude Unmanned Aerial Vehicles as a Tool for the Remediation of Radiologically Contaminated Environments. 1-13. Paper presented at WM2016, Phoenix, Arizona, United Kingdom.

Peer reviewed version

Link to publication record in Explore Bristol Research
PDF-document

University of Bristol - Explore Bristol Research
General rights

Low-Altitude Unmanned Aerial Vehicles as a Tool for the Remediation of Radiologically Contaminated Environments – 16257.

Peter G. Martin *, Thomas B. Scott *, Oliver D. Payton *, David A. Richards *, Yosuke Yamashiki **, John S. Fardoulis *
* University of Bristol, UK, BS8 1TH
** University of Kyoto, Japan, 606-8501

ABSTRACT

Following the events at the Fukushima Daiichi Nuclear Power Plant (FDNPP) in March 2011, significant quantities of radioactive material were released into the local Japanese as well as the wider global environment. At the fifth anniversary of the incident, much work and expense is still being dedicated to the remediation of a large area of eastern Japan, contaminated primarily with radio-caesium. Due to the complex topography of the geographical area of Japan effected, it is important to understand contaminant evolution/migration at the greatest possible resolution – previous methods have lacked this.

An increase in the spatial resolution of radiation mapping over other previous methods has been achieved through the deployment of an unmanned aerial vehicle (UAV). The platform used during this work combined a low-altitude multi-rotor UAV with a lightweight radiation mapping system to achieve sub-meter resolution. Using this system it was possible to measure the distribution of radionuclide contamination at a number of sites within the Fukushima Prefecture region of Japan. Unlike ground-based surveys conducted on foot by humans that attain a comparable resolution, such a system eliminates the potentially significant dose that would otherwise be received, as well as the influence of shielding on results.

In addition to providing a rapid and high resolution response to radiological incidents, such monitoring technology has the potential to be a powerful tool in post-operational clean-out (POCO) at nuclear sites undergoing decommissioning worldwide.

INTRODUCTION

Incident Background

At 14:46pm on 11th March 2011, the magnitude 9.0 Great Tōhoku Earthquake occurred 70 km off the eastern coast of Japan [1]. Immediately after the seismic activity, all four of the operating reactors at the site entered a SCRAM – with the insertion of control rods and initialisation of emergency core cooling to lower the temperature within the reactor pressure vessel (RPV). However, 50 minutes after this shutdown, a 15 meter high tsunami arrived at the coastal site – overtopping the tsunami defence walls. The water immediately inundated the plant, destroying pylons

that provided power to the cooling systems, as well as flooding the basement levels within the reactor halls supplying final backup battery power.

The reactors at the Fukushima site were all boiling water reactors (BWR), constructed by General Electric, Toshiba and Hitachi with Mark I containment systems to protect against the energy released by a loss-of-coolant accident (LOCA). At the time of the event, only 3 of the 6 reactors at the site were in operation; reactors 1, 2 and 3, with reactor 4 undergoing planned maintenance and reactors 5 and 6 in an extended period of cold-shutdown.

Despite intense efforts by the plant operators, Tokyo Electric Power Company Inc. (TEPCO) after the incident, over the succeeding three days, a series of large explosions impacted the site, with the release of significant quantities of radionuclides into the surrounding environment. Early estimates place the total quantity of radioactivity released at 340 to 800 PBq [2], with the majority consisting of volatile noble and fission product gases such as Xe-133, I-131, Cs-134 and Cs-137 [3,4].

Large Area Aerial Radiation Mapping Systems

The application of aerial systems to identify and map radiological intensity on the ground is a mature technique, having been previously extensively employed for both natural [5] and anthropogenic sites [6]. Typically, these radiation surveys use large volume detectors (1 l to >50 l for high-sensitivity spectrometric surveys) such as thallium-activated sodium iodide (NaI(TI)) [5,6], weighing in excess of 200 kg, attached to large helicopters or fixed-wing aircraft [7–11]. Whilst able to cover considerable areas over short durations, limitations of these surveys exist when trying to collect high spatial resolution data due to the high relative ground speeds and altitudes at which they must operate; with resolutions averaging upwards in excess of 300 m [9]. In addition to the low resolution achieved, the use of helicopter or fixed-wing systems have the further drawback of their great financial expense, not only with respect to the initial outlay on both the aircraft and associated detection system, but also the requirement for well-trained pilots and maintenance teams for their successful operation.

Post-Incident Radiation Monitoring

Following the release of radioactivity at Fukushima, no mapping of the contamination spread was conducted for 11 days. Finally on the 22nd March 2011 exploratory mapping was conducted by the Ministry of Education, Culture, Sports, Science and Technology (MEXT) in collaboration with the US DOE [12] using manned helicopters at altitudes of 150-700 m, producing a rapid depiction of the dispersion of the radiation.

In order to provide greater assistance with the remediation efforts as well as better understanding the spread and eventual fate of the contamination within the environment, work was conducted to improve on the low spatial resolution already obtained. This increase in resolution was achieved by Sanada et al [13] using a 94 kg unmanned helicopter more commonly used for agricultural crop-dusting -

equipped with three LaBr$_3$:Ce detectors totalling 6.5 kg, mounted to the underside of the aircraft. Mapping was conducted at a reduced altitude of 80 m and a maximum velocity of 8 m/s, to yield a typical pixel size of 25 m². However, this method was still incomparable to the resolution that is achievable through the use of ground-based monitoring conducted by humans.

Additional improvements to the resolution achievable have been brought about through the use of remotely operated UAVs in response to the incident at the FDNPP, such as work by MacFarlane et al [14], described below.

METHOD

Unmanned Aerial Vehicle

The current UAV used in this and previous work was designed and constructed at the University of Bristol, UK – with the initial system described in MacFarlane et al [14]. For increased efficiency, resilience and total duration flight time, an X8 multirotor configuration has since been employed (Fig. 1.), consisting of a cross-shaped airframe with brushless electric motors mounted both above and below the carbon-fibre arms. With propellers installed, the aircraft was 1.3 m in diameter, with a height of 0.5 m and weighing 7.0 kg when carrying the two lithium polymer (LiPo) batteries required to power the system. The use of LiPo batteries provided a typical flight time of 30 – 35 minutes per full charge, depending on the operations performed. Unlike other, more conventional UAVs, the use of a dual layer setup offers a critical layer of redundancy should one, or multiple, motors or propellers fail.

Control of the system was performed by the open-source Arducopter (APM version 2.6) autopilot system (diydrones.com). Whilst both take-off and landing of the UAV were performed manually, using typical handheld remote controls – once airborne, the UAV executed predetermined flightpaths using preselected waypoints and altitudes. To ensure accurate positioning of the UAV, an on-board high frequency (10 Hz refresh) GPS unit was coupled with a barometric pressure sensor, both of which inputted directly into the flight control system. Mounted directly under the front of the system was a small, lightweight camera that enabled the operator to monitor the progress of the flight as well as assisting with the remote piloting of the craft.

Radiation Detection and Measurement

Unlike previous systems employed to determine radiological contamination, the spatial measurements of radiological intensity in this and other earlier work by Martin et al [15,16] have been conducted using a lightweight gamma-ray spectrometer with a small volume (1 cm³) uncollimated cadmium zinc telluride (CZT) coplanar-grid detector and a 4096 channel MCA from Kromek™ Ltd. (GR1, Kromek, County Durham, UK).
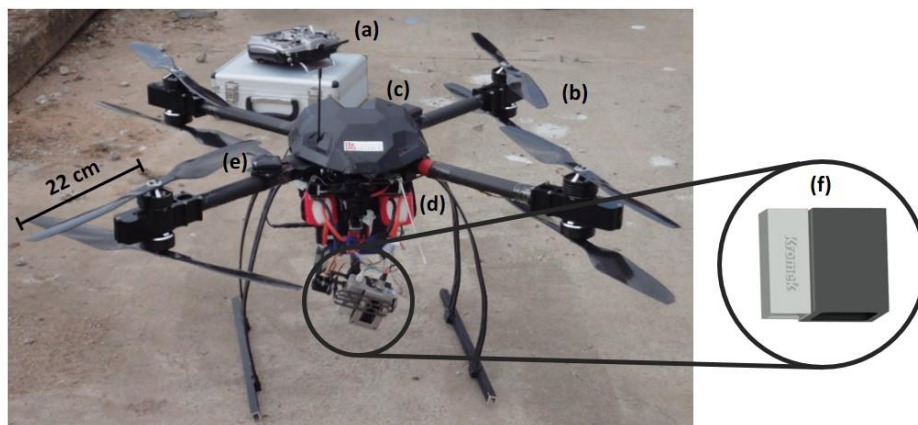
Fig. 1. Image of the UAV radiation mapping system developed at the University of Bristol (modified from [16]): (a) remote control unit, (b) counter-rotating carbon fibre propellers, (c) plastic cover over flight control system, (d) lithium polymer batteries, (e) GPS unit and (f) detection system consisting of side mounted micro gamma-spectrometer (left) and single-point laser rangefinder (right).

Like many standard detection materials, the energy measurement range of the micro-spectrometer was 30 keV to 3.0 MeV, with an energy resolution of <2.5% FWHM at 662 keV. The electrical noise on the detector was <10 keV Full Width at Half Maximum (FWHM) [17].

In addition to the gamma-spectrometer, below the UAV was also mounted a single-point high-accuracy (<5 cm at 30 m) laser rangefinder by Acuity™ [18]. The converging data streams from these two devices as well as from an additional GPS unit mounted onto the UAV were collated onto an Arduino™ Mega ADK microcontroller (Scarmagno, Italy) where the data was recorded in real time onto the boards SD card in addition to being transmitted by radio as an encrypted data-stream in near real-time (0.5 second delay) to a nearby base-station. Data was sampled at a rate of 2 Hz using this system.

Both the gamma-spectrometer and rangefinder unit were mounted side-by-side onto a three-axis active gimballed stage to keep both normal to the ground surface, irrespective of the position and attitude of the aircraft.

For radiation mapping, flights were carried out at a velocity of 1 ms^{-1}, with the UAV maintained at a constant altitude of 1-5 m above surfaces (trees, fields, and roofs) in order to avoid collisions with obstacles. During all radiation mapping, a constant grid-separation of 1.5 m was maintained whenever practicable, dependent on terrain and obstructions.

The calibration of the detector system to allow for conversion between counts per second (cps) and dose (μSv/h) was performed with an automatically-calibrating SAM 940 Defender sodium iodide detector (Berkeley Nucleonics Corporation, California, USA). A variety of sources with documented activities were positioned at assorted

distances from both detectors within the lab for a calibration constant to be determined – a series of comparisons within the field between the values obtained by both detection systems insured consistent calibration.

A number of differing localities located within the fallout affected region were used in the deployment of the system. Location 1, a former rice paddy field located on the outskirts of Kawamata Town [37.6065N, 140.6072E] was mildly contaminated by the release from the FDNPP, but has since been stripped and is now the site for the storage of contaminated material removed from elsewhere locally in the Fukushima Prefecture, stored in 1 m³ black bags. Location 2, located north east of Location 1, is a series of unremediated fields within Iitate Village [37.6154N, 140.7097E] formerly used for different types of agricultural crops, a road dissects the centre of the site. Location 3 is also agricultural land, used for the production of rice, also within the Kawamata region of Fukushima Prefecture [37.5887N, 140.7011E], unlike the former two sites – this locality consists of a series of small fields cut into the side of a hillside forming a stepped site. Like Location 2, this site had also not been the subject of any remediation efforts prior to this study. Data presented within this work was collected during fieldwork undertaken during May 2014 and October 2015, and are identified accordingly.

Data Analysis

Processing of radiation contamination data collected by the UAV was conducted using custom-built software produced at the University of Bristol, detailed fully within [15,16]. Radiation intensity maps were produced whereby a scaled coloured overlay depicted the calculated radiation intensity across the entire energy range (30 keV – 3.0 MeV) at measured positions on the map. Each of the data points consisted of a value from the rangefinder, a GPS latitude and longitude of the device as well as a full gamma spectrum from the region. For each of the measurement points collected at 0.5 second intervals, the data was normalised to a height of 1 m via measurements obtained using the rangefinder, with the possible source area on the ground existing as a function of both the aperture of the detector and its height above ground. The full gamma spectrum for each of the data points was condensed into a cps value.

The process of normalising data from collection altitude to a height of 1 m in order to produce contamination maps was conducted following the inverse square law calculation of radiation distribution from a point source [14]. Overlapping measurements were averaged, with this value used for plotting. During previous airborne surveys, performed at greater altitudes of 50 – 250 m using helicopters and fixed-wing systems [19–21], an exponential fall-off in the detected level of radiation was employed to normalise measurements to ground level. However, following from earlier work [14,15], it was determined that data arising from these lower altitude surveys (1 – 10 m) better conforms to an inverse square relationship of radiation intensity with height. This inverse square relationship was established through undertaking a series of readings at numerous heights above the ground surface (up to 15 m) across a range of sites both within the affected region in Japan as well

at a similarly contaminated site in Cornwall, England [15] using both the Kromek™ GR1 and the SAM 940 Defender.

3D Radiation Mapping

In addition to producing 2-dimensional radiation maps of a surface overflown by the UAV, the use of a 3D scanning Lidar has allowed development of 3-dimensional radiation maps, to provide a greater visual representation of contamination.

After conducting survey flights as described above using the UAV with the associated radiation mapping payload, subsequent, low altitude flights were performed with the Lidar unit mounted under the aircraft following the same flight paths to generate a 3D point-cloud. The 3D scanning Lidar unit used during this work was a UAV LidarPod® (Routescene®, Mapix Technologies, Edinburgh, UK) based upon the Velodyne® (Morgan Hill, California, USA) HDL-32E Lidar unit. Attached directly to the underside of the UAV, the LidarPod weighs 2.5 kg including the instrument and associated hardware. The cylindrical LidarPod has dimensions of 320 mm (length) and 100 mm (diameter), collecting 700,000 3D points per second with 32 x 905 nm eye safe laser sensor / detector pairs. Capable of flight times of 20 minutes on the UAV, the laser system has absolute position accuracy of 0.04 m at 20 m range or 0.06 m at 40 m range. Position referencing of the Lidar unit and the generated point-cloud was achieved through the use of high accuracy differential dGPS and an inertial navigation system (INS). This d-GPS and INS system combined temperature calibrated accelerometers, gyroscopes and magnetometers with multiple satellite navigation systems (GPS, GLONASS, GALILEO and BeiDou) to position the LidarPod with a horizontal accuracy of 0.008 m and 0.015 m in the vertical.

RESULTS AND DISCUSSION

The radiation contamination maps obtained for each of the three localities studied are presented below (Figs. 2 – 4). For each of these sites, areas of elevated radioactivity are present over previously measured values [22].

Location 1

The distribution of radioactivity at Location 1 is shown in Fig. 2. (a) with the corresponding aerial photograph of the site in Fig. 2. (b). Apparent regions of heightened activity approaching 1.7 µSv/h are seen to correlate with the position of the black storage bags containing contaminated material removed from elsewhere within the plume affected area. A background level across the site of 0.1 to 0.15 µSv/h is seen on the land surrounding the storage bags where material contaminated to low levels had been previously removed to prepare the site. Although containing contaminated material in large 1 m³ volumes, the dose rate emanating from these containers is low when compared to other sites (Locations 2 and 3) located closer to the FDNPP, likely due to the considerable level of self-shielding provided by the material itself.
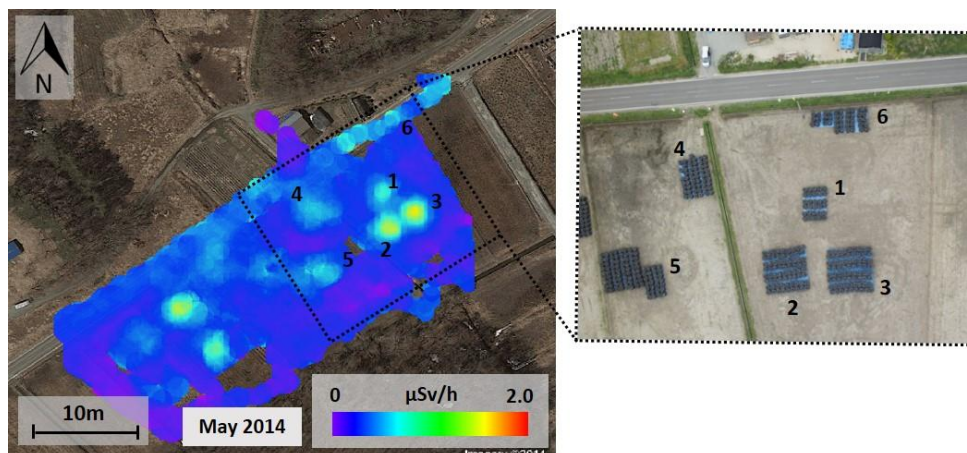
Fig. 2. (a) Radiation distribution map of Location 1, a bail storage site and (b) an aerial image taken over the site with features identified.

Location 2

Unlike Location 1, Location 2 represents a site where considerably more radiological contamination occurred. Because of this, less effort has been devoted to its remediation, other than allowing natural decay to reduce radioactivity levels. Fig. 3. (a) shows the radiation contamination map produced of the site during May 2014, with the same site surveyed during October 2015, Fig. 3. (b). Visible from the data collected during May 2014 (Fig. 3. (a)) is the near uniform distribution of contamination across the entire site, with the road dissecting the centre of the locality displaying approximately half the dose rate of the neighbouring fields. This reduction is likely attributable to precipitation removing contaminant species from the hard road surface - redepositing them onto the surrounding fields, instead of road cleaning which was not occurring in such higher activity regions. Higher levels of activity are observed in the southern-most field where corn-based crops were planted, in contrast to the field to the north of the road where a lower activity is observed in a field in which rice was planted. This difference likely illustrates the ability of different crop species to capture and accumulate fallout material.

At the time of study in October 2015, remediation work had commenced at the site as part of the ongoing clean-up operations – with the highlighted areas having seen decontamination work. The field to the south of the road had not received any action, with the reduction in activity a result of natural radioactive decay. Extensive daily scrubbing around the Iitate area has seen the activity on the road surfaces reduced markedly to below 1.4 µSv/h. Apparent to the north-east of the site is a region of elevated intensity (5.6 µSv/h) relative to the surroundings, representing the location of a bail store of material removed from the across the site.
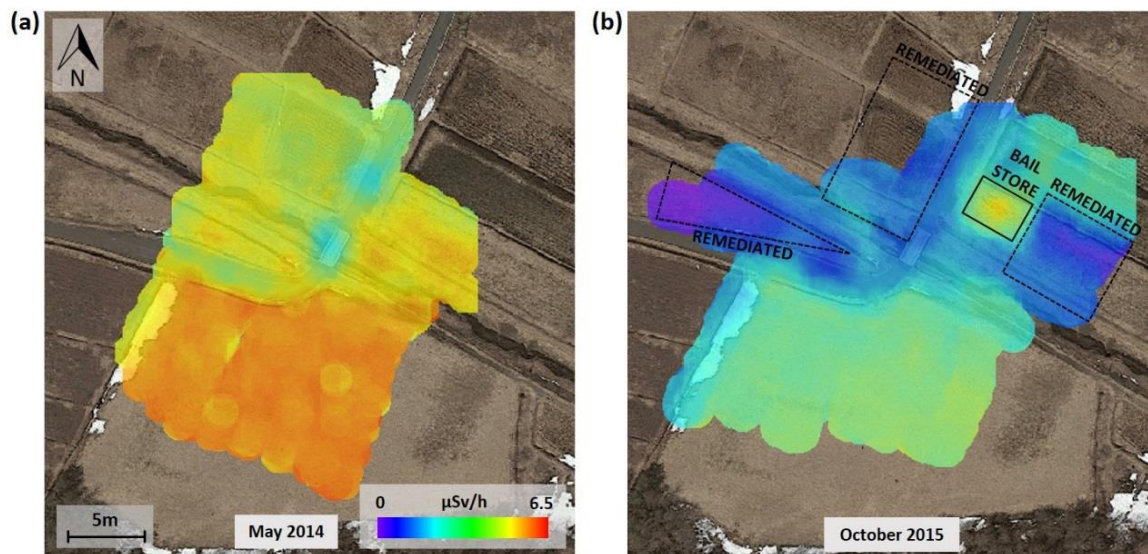
Fig. 3. Radiation intensity distribution maps taken from Iitate (Location 2), displayed as normalised to 1 m above the ground surface in dose rate (μSv/h), (a) taken in May 2014 and (b) the same site surveyed later during October 2015.

Location 3

As at Location 2, Location 3 represents a site that was affected by similar levels of contamination as Location 2 and had also yet to receive any remediation work. Unlike the two former sites, this location was not flat, but consisted of several small, flat surfaces cut into the side of a slope along with a series of drainage channels. The radiation contamination map of the site is shown in Fig. 4. (a); apparent from this map, the distribution of radioactivity within this site is not as consistent as that of Location 2. Across the majority of the site, the measured dose rate is <2 μSv/h, however, there exists points during the survey at which the dose rate reaches >6.0 μSv/h. These high activity points correspond to drainage ditches around the site, where dense contaminant material is deposited. Over time, it is anticipated that this material will eventually progress southwards, downslope.

Additional visualisation of the radioactivity on the site was performed through interrogation of the raw data produced by the radiation mapping system. A topographic surface generated by subtracting height data acquired by the single-point rangefinder from altitude data acquired by the on-board GPS unit; onto this surface is overlain radiological data, as shown in Fig. 4. (b).
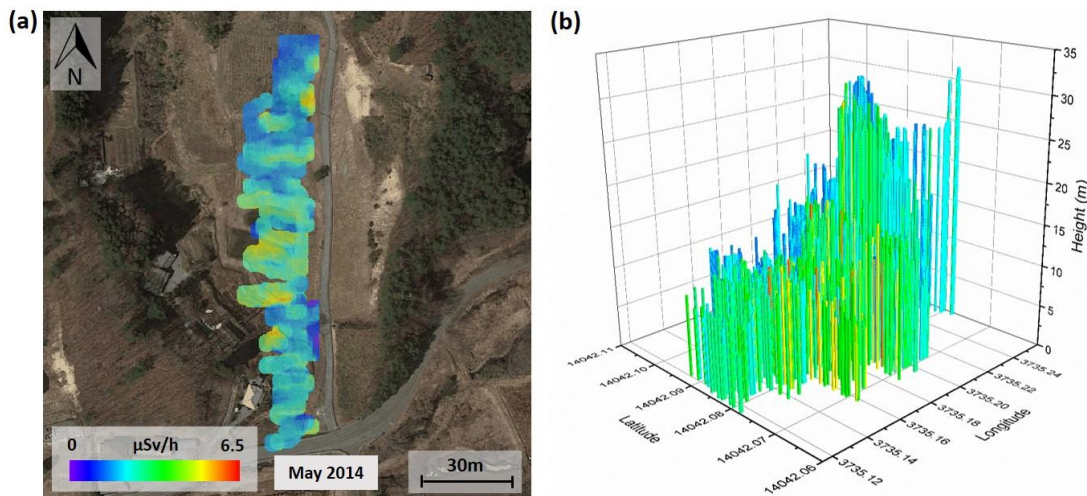
Fig. 4. (a) Radiation intensity distribution map taken from Location 3, displayed as normalised to 1 m above the ground surface in dose rate (µSv/h) and (b) a 3D contamination map produced through overlaying radiation intensity data onto a surface produced through the interpolation of data from the laser rangefinder and GPS.

The accumulation of activity within the drainage network at Location 3 is also depicted within Fig. 4. (b), where depressions are seen to display increased count rate and dose.

Gamma-Spectrometry

As well as determining the count and dose rate across each of the localities, the use of the CZT detector allows the isotopic fingerprint of the contamination to be examined. The gamma spectra of the contamination arising from the entire area of each of the three localities is shown in Fig. 5. Each of the spectra are identical with respect to the peaks produced; with peaks at the energies corresponding to the known contaminants of Cs-134 and Cs-137, but with differing intensities dependant on the activity of the site.

3D Radiation Mapping

Whereas Fig. 4. (b) provided a digital elevation model (DEM) of the site using data interpolated from the radiation detection system, containing only a single range-finding laser, the use of the dedicated 3D scanning Lidar unit produced a higher resolution topographic DEM, onto which radiological data can be overlain.

A portion of the topographic model produced by the LidarPod® UAV mounted system at a further bail storage site within Kawamata Town, is shown in Fig. 6. On the ground surface of the site, which had been cleaned extensively prior to the placement of the 1 m³ storage bags, shows a correspondingly negligible activity, at levels of 0.1 to 0.2 µSv/h - similar to those observed at Location 1 (Fig. 2). The increased activity of the

storage bags in relation to the ground is apparent, with a typical dose rate of 1.2 µSv/h measured with the system. Again, this level of activity measured from the bags represents elevated levels of radiation when compared to previous background levels [22], however, these levels are much lower than other localities within the Fukushima Prefecture that have not been the subject of any remedial works.
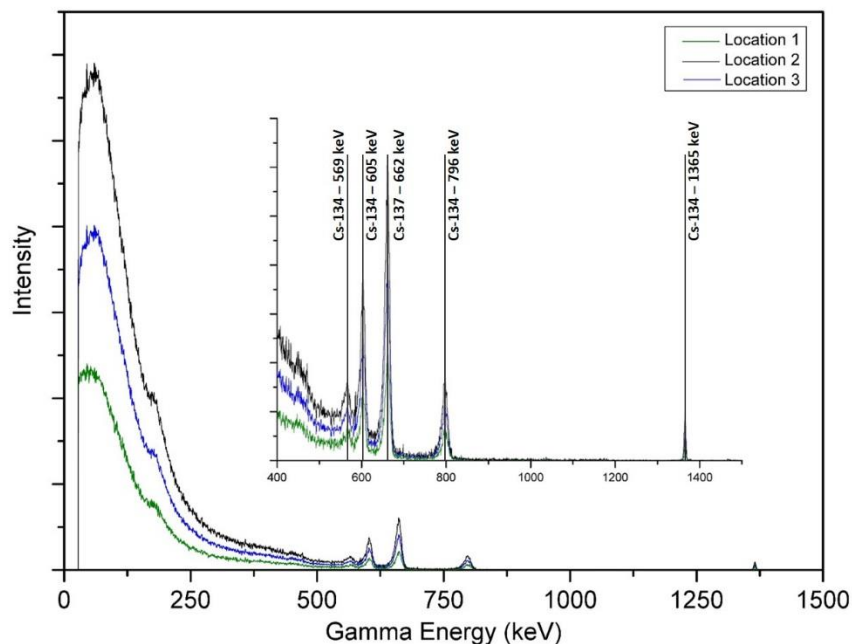

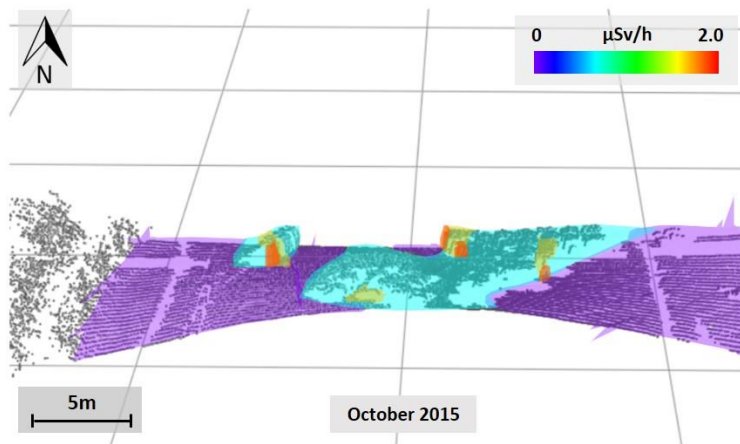**Fig. 5.** Gamma spectrum produced at each of the localities with peaks identified.

Fig. 6. Topographic model produced using a 3D scanning Lidar mounted to the underside of the UAV overlain with measured radiation intensity data.

CONCLUSION

The work presented demonstrates the application of a small, unmanned aerial vehicle for the mapping of radioactively contaminated sites within the Fukushima Prefecture region of eastern Japan. Using this system it was possible to attain spatial resolution of less than 1 m, a great improvement over other previously employed airborne techniques. Deploying this instrument into such an environment, it is possible to undertake contamination surveys where not previously possible or practicable; such as sites with limited or difficult access or those into which it is not desirable to send humans.

As well as identifying regions within a site with heightened contamination, the analysis of the gamma-energy spectra captured by the instrument during flights, allows for the identification of the contributing radionuclides – a key factor in dictating the most appropriate remediation methods and disposal route of contaminated material.

In addition to the primary advantages of this system of the improved spatial resolution and reduced dose to those conducting the survey, further advantages include its straightforward upkeep and operation as well as its portability and rapid deployability. The cost of such a system is also advantageous to its selection over large, fixed-wing and helicopter systems. However, disadvantages of multi-rotor systems at the present time are their shorter flight times when compared to larger aerial vehicles, as well as their inability to operate outside of calm weather conditions and the need to conduct work using a small, lightweight sensor.

Though still in its initial development stages, the combination of high-resolution radiation mapping, coupled with 3D scanning Lidar topographic models to produce 3-dimensional radiation maps appears a powerful method to visualise the distribution of radiological contamination. Through the application of particle transport modelling to larger scale 3-dimensional radiation maps it would be possible to predict the transport and eventual fate of material within the environment as a function of naturally occurring processes.

Although invaluable in the mapping of sites contaminated after an incident such as that at the FDNPP, the use of unmanned aerial vehicles for radiation mapping could provide a powerful tool with numerous application for tasks such as routine surveys and monitoring at nuclear sites worldwide.

REFERENCES

1. M. Simons, S.E. Minson, A. Sladen, F. Ortega, J. Jiang, S.E. Owen, et al., *The 2011 magnitude 9.0 Tohoku-Oki earthquake: mosaicking the megathrust from seconds to centuries.*, Science. **332** (2011): p. 1421-1425.

2. G. Steinhauser, A. Brandl, T.E. Johnson, *Comparison of the Chernobyl and Fukushima nuclear accidents: a review of the environmental impacts.*, Sci. Total Environ. **470-471** (2014): p. 800-817.
3. M. Chino, H. Nakayama, H. Nagai, H. Terada, G. Katata, H. Yamazawa, *Preliminary estimation of release amounts of 131I and 137Cs accidentally discharged from the Fukushima Daiichi nuclear power plant into the atmosphere*, J. Nucl. Sci. Technol. **48**(7) (2011): p. 1129-1134.
4. A. Stohl, P. Seibert, G. Wotawa, D. Arnold, J.F. Burkhart, S. Eckhardt, et al., *Xenon-133 and caesium-137 releases into the atmosphere from the Fukushima Dai-ichi nuclear power plant: determination of the source term, atmospheric dispersion and deposition*, Atmos. Chem. Phys. **12** (2012): p. 2313-2343.
5. D. Beamish, *Environmental radioactivity in the UK: the airborne geophysical view of dose rate estimates.*, J. Environ. Radioact. **138** (2014): p. 249-263.
6. K. Kurvinen, P. Smolander, R. Pöllänen, S. Kuukankorpi, M. Kettunen, J. Lyytinen, *Design of a radiation surveillance unit for an unmanned aerial vehicle.*, J. Environ. Radioact. **81** (2005): p. 1-10.
7. G.F. Schwarz, L. Rybach, C.K. Barlocher, E.E. Klingele, *Development and calibration of an airborne radiometric measuring system*, IAEA TECDOC-**827**. (1995): p. 26-35.
8. G.F. Schwarz, L. Rybach, E.E. Klingele, *Data processing and mapping in airborne radioactivity surveys*, IAEA TECDOC-**827**. (1995): p. 61-70.
9. D.C.W. Sanderson, J.D. Allyson, A.N. Tyler, E.M. Scott, *Environmental applications of airborne gamma spectrometry*, IAEA TECDOC-**827**. (1995): p. 71–91.
10. H. Mellander, *The role of mobile gamma spectrometry in the Swedish emergency response programme for nuclear accidents - experience and future plans*, IAEA TECDOC-**827**. (1995): p. 187-195.
11. S. Okuyama, T. Torii, A. Suzuki, M. Shibuya, N. Miyazaki, *A Remote Radiation Monitoring System Using an Autonomous Unmanned Helicopter for Nuclear Emergencies*, J. Nucl. Sci. Technol. **45** (2014): p. 414-416.
12. U.S. Department of Energy and NNSA. *Radiological Assessment March 22, 2011.* http://energy.gov/situation-japan-updated-12513 (accessed Dec 12, 2015).
13. Y. Sanada, A. Kondo, T. Sugita, T. Torii, *Distribution of radioactive cesium measured by aerial radiation monitoring*, Hoshasen. **38**(3) (2012): p. 137-140.
14. J.W. MacFarlane, O.D. Payton, A.C. Keatley, G.P.T. Scott, H. Pullin, R.A. Crane, et al., *Lightweight aerial vehicles for monitoring, assessment and mapping of radiation anomalies.*, J. Environ. Radioact. **136** (2014): p. 127-130.
15. P.G. Martin, O.D. Payton, J.S. Fardoulis, D.A. Richards, T.B. Scott, *The use of unmanned aerial systems for the mapping of legacy uranium mines*, J. Environ. Radioact. **143** (2015): p. 135-140.
16. P.G. Martin, O.D. Payton, J.S. Fardoulis, D.A. Richards, Y. Yamashiki, T.B. Scott, *Low altitude unmanned aerial vehicle for characterising remediation effectiveness following the FDNPP accident*, J. Environ. Radioact. **151** (2016): p. 58-63.
17. Kromek Group PLC, GR1 Spec Sheet; Revision 10, (2015). www.kromek.com/products_gr1spectrometer.asp (accessed June 23, 2015).
18. AR2500 Acuity™, Acuity AR2500 Specification. www.acuitylaser.com (accessed June 3, 2015).

19. B.R.S. Minty, *Fundamental of airborne gamma-ray spectrometry*, J. Aust. Geol. Geophys. **17** (1997): p. 39-50.
20. B.R.S. Minty, A.P.J. Luyendyk, R.C. Brodie, *Calibration and data processing for airborne gamma-ray spectrometry*, J. Aust. Geol. Geophys. **17** (1997): p. 51-62.
21. Y. Sanada, T. Sugita, Y. Nishizawa, A. Kondo, T. Torii, *The aerial radiation monitoring in Japan after the Fukushima Daiichi nuclear power plant accident*, Prog. Nucl. Sci. Technol. **4** (2014): p. 76-80.
22. S. Abe, K. Fujitaka, M. Abe, K. Fujimoto, *Extensive Field Survey of Natural Radiation in Japan*, J. Nucl. Sci. Technol. **18** (1981): p. 21-45.